

Enhanced light absorption and through-thickness heat conduction of vertically aligned transferable carbon nanotube/silicone rubber composite films

Michael Dasbach^a, Norbert A. Hampp^{a,b,*}

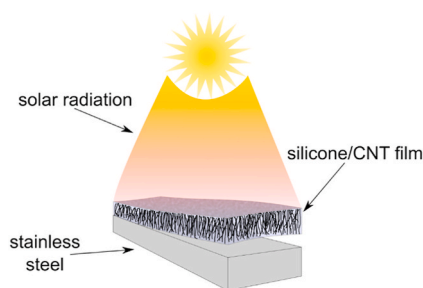
^a Department of Chemistry, Philipps-University of Marburg, Hans-Meerwein-Str. 4, 35032, Marburg, Germany

^b Material Science Center, 35032, Marburg, Germany

HIGHLIGHTS

- Various multi-walled carbon nanotubes were generated on laser-treated stainless steel.
- Vertically aligned carbon nanotube (CNT) arrays provide broadband light absorption with low reflection.
- Silicone embedding of CNT leads to polymeric films with preserved high order of the CNTs.
- The films can be transferred to any other surface without losing their internal anisotropic structure.

GRAPHICAL ABSTRACT



ARTICLE INFO

Keywords:

Carbon nanotubes
Silicone embedding
Transferable film
Light absorption
Anisotropic heat conduction

ABSTRACT

Easily manageable flexible films of multi-walled carbon nanotubes (MWCNT) were prepared and characterized. For the preparation of the MWCNTs pulsed laser-induced dewetting (PLiD) of stainless steel surfaces is employed to generate freely designable arrays of catalytic nanoparticles (NP), which facilitate the MWCNT growth in a chemical vapor deposition (CVD) process. The density of the NP fields, and thus the areal density of the CNTs grown, can be controlled through the used laser parameters. As prepared CNT-arrays were soaked with silicone and cross-linked to form a flexible detachable film that may be reattached onto any other surface. The silicone matrix increases reflection only minimally by about 2%. The vertically aligned CNT (VACNT) arrays were undisturbed during capillary filling of silicone. The anisotropic heat transfer properties of the VACNTs are preserved. Such films are excellent light-absorbers and e.g. may enhance the effectiveness of solar panels or transfer heat from microprocessors to a cooling system.

1. Introduction

The growing industrialization of the world economy, as well as the increasing environmental pollution, leads to rising demand for so-called

clean energy devices. Solar energy usage, due to its high accessibility and low environmental impact, is one of the leading technology branches for this kind of application.

CNTs have been used to reinforce various materials [1–4], among

* Corresponding author. Department of Chemistry, Philipps-University of Marburg, Hans-Meerwein-Str. 4, 35032, Marburg, Germany.

E-mail address: hampp@uni-marburg.de (N.A. Hampp).

<https://doi.org/10.1016/j.matchemphys.2021.124690>

Received 9 February 2021; Received in revised form 21 April 2021; Accepted 22 April 2021

Available online 28 April 2021

0254-0584/© 2021 Elsevier B.V. All rights reserved.

them silicone [5], but the alignment of the CNTs is not essential for such applications. CNT as active electronic elements, e.g. field emission, require a high degree of alignment and embedding into an insulator. This has been realized by lithographic methods quite early [6]. CNTs show good optical absorber qualities over a wide band of wavelengths due to their π -band optical transition, as it is known for other high-absorption materials, such as carbon black or graphite [7]. Due to their electronic and optical properties CNTs are interesting materials for light absorption applications [8–11], because of their ability to tune their bandgaps over a broad wavelength range [12] and their high carrier mobility along their long axis [13,14]. In particular, vertically aligned carbon nanotubes (VACNT) [15–18] due to their morphologically determined high amount of microcavities offer ideal conditions for light trapping resulting in a high absorption behavior [19].

There is one problem in the use of VACNT, which is that the VACNT need to be grown directly on the substrate to obtain vertical alignment.

In this study, we want to investigate the function of the light absorption potential of different MWCNT-layer morphologies on stainless steel. In recent studies we demonstrated the potential of laser-induced particle generation for CVD-based CNT growth, providing the possibility of growing CNTs with all kinds of morphologies [20,21]. Silicone soaking and cross-linking of the CNT-arrays result in mechanically stable, easily useable CNT films, which can be detached from the growth substrate and reattached to merely any other surface, still preserving their light absorption properties and the anisotropic alignment of the CNTs.

2. Materials and method

Yacht polished stainless steel AISI 304 (EN AW 1.4301) was used as a substrate for catalyst generation for the CNT studies. Flow cells were prepared of the same steel in-house. A frequency-doubled nanosecond pulsed Nd:YVO₄-laser, emitting laser pulses of 5 ns pulse width at a wavelength of 532 nm (Explorer XP 532–5, Newport, USA), was used for catalyst precursor formation. The laser beam was scanned over the stainless steel samples by a galvanometer scan head (SCANgine 14–532, Scanlab, Germany), equipped with an F-Theta lens (Rodenstock, $f = 163$ mm, Germany), focused to a spot diameter of 100 μm ($1/e^2$). A line spacing of 3 μm , a pulse repetition rate of $f = 50$ KHz, a fluence per pulse of $\Phi = 0.34$ J cm^{-2} , and scan speeds from $v = 1.3$ mm s^{-1} up to $v = 200$ mm s^{-1} were used to control pulse overlaps and thus the number of dewetting cycles (DC) applied, which ranged from DC = 639 up to DC = 115,007. For CNT growth the samples were placed in a horizontal quartz glass furnace (35 mm inner diameter, 150 mm heating zone) at 750 °C with a heating rate of 16 °C min^{-1} . Hydrostar 10 (Ar/H₂ 90/10; 100 L h^{-1}) was used as the carrier gas and ethylene gas (6 L h^{-1}) was added for 10 min as the precursor for CNT growth. Samples were placed at a downstream furnace position to achieve optimal growth conditions. For silicone/CNT-film preparation, the CNT samples were brought into contact at one edge with a silicone two-component mixture (Sylgard 184, 10:1). The silicone soaks itself into the CNT sample due to the high capillary forces of the CNT structure despite the relatively high viscosity of the silicone. Illumination for the light absorption studies was done in a Suntest XLS+ (Ametek, USA) with a radiation fluence of $\Phi = 250$ –765 $\text{J s}^{-1} \text{m}^{-2}$. For temperature measurement, PT100 temperature sensors were used. Dynamic measurements were done in homemade flow cells of 35 × 25 × 10 mm dimension, with an inner tube diameter of 3 mm. Flow cells had a capacity of 0.8 mL and a total volume of 30 mL water was in the whole circle. The flow rate was set to 35 mL min^{-1} . For reattachment studies of the film, the film was simply cut off the substrate with a razor blade. Afterward, the film was pressed onto a stainless steel surface by a glass plate to omit any entrapped air between steel and silicone/CNT film. UV-Vis measurements were recorded on a Lambda 1050 (PerkinElmer, USA). For SEM images a Gemini II (Zeiss, Germany) was used.

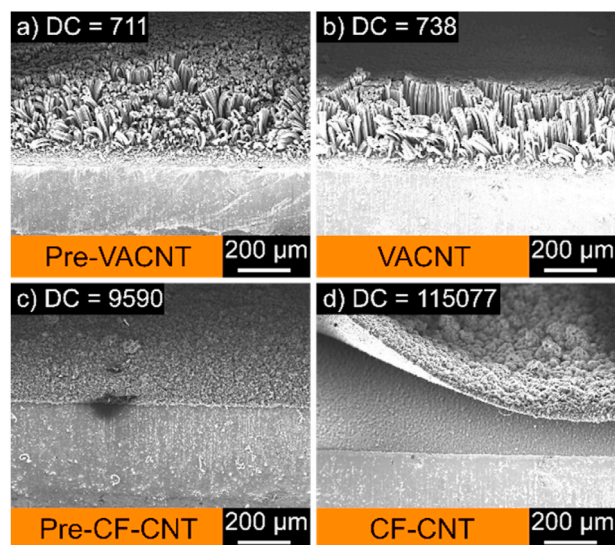


Fig. 1. Electron microscopy of cross-sections of CNT arrays generated by constant laser pulse fluence ($\Phi = 0.34$ J cm^{-2}) but various numbers of DCs. a) CNT-array created using a DC number close but below where vertical alignment of CNTs is obtained (Pre-VACNTs), b) VACNTs, c) beginning of cauliflower-like growth (Pre-CF-CNT), and finally d) CF-CNTs.

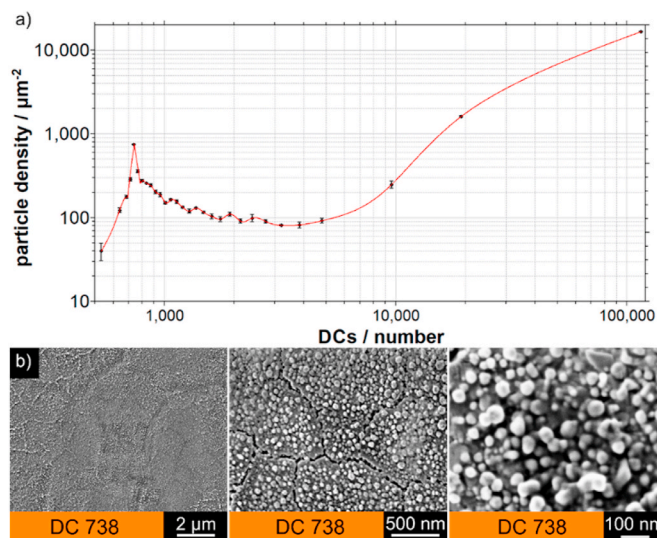


Fig. 2. (a) Particle density depending on the number of DCs. A rather sharp optimum at DC = 738 is observed for the laser parameters used. (b) Density and morphology of the prepared NPs.

3. Results and discussion

Laser treatment of stainless steel in air results in transient surface melting, provoking an unstable surface state, which relaxes by dewetting the liquefied metal film accompanied by the formation of metal oxide NP. The size and the areal density of those nanoparticles can be precisely tuned by adjusting the laser pulse fluence and the number of DCs applied, as both directly define the CNT morphology during CVD growth. The morphology of the CNTs may be tuned from Pre-VACNTs, over VACNTs, to CF-CNTs (cauliflower CNTs), as shown in Fig. 1.

The low areal density of NPs results in partially stabilized CNT growth (Fig. 1a, DC = 711). A slightly higher NP density, resulting from 738 DCs, leads to CNTs that can support themselves to form vertical alignment (Fig. 1b). Massive laser treatment results in the structuring of the surface, accompanied by a large amount of NPs on a non-flat surface,

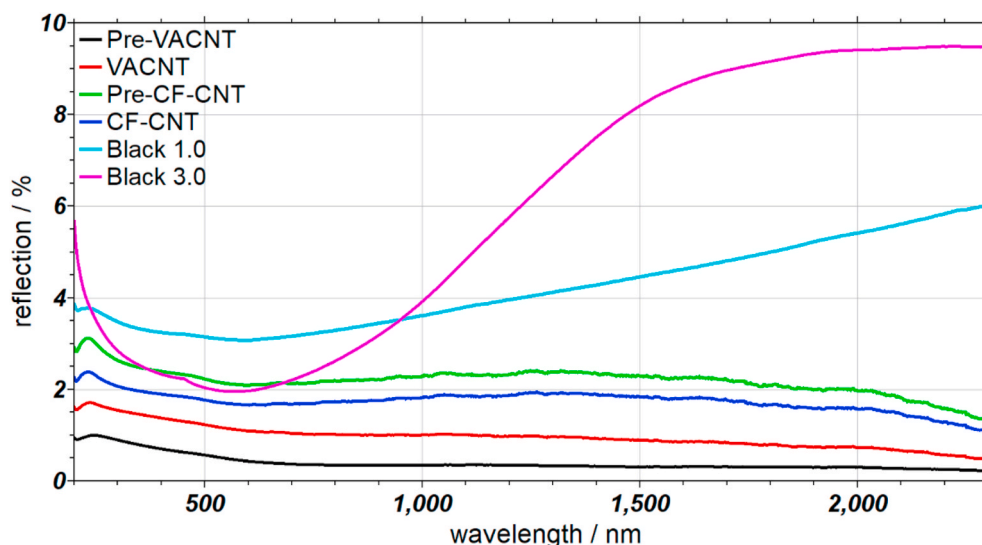


Fig. 3. UV-Vis-NIR reflection spectra of CNT-samples under vertical light incidence. For the morphology of the samples compare to Fig. 1. For comparison two commercially available black carbon-based acrylic paints, i.e. Black 1.0 and 3.0, are shown. (In the Supplementary Information reflection spectra of more samples are shown in Figure SI4).

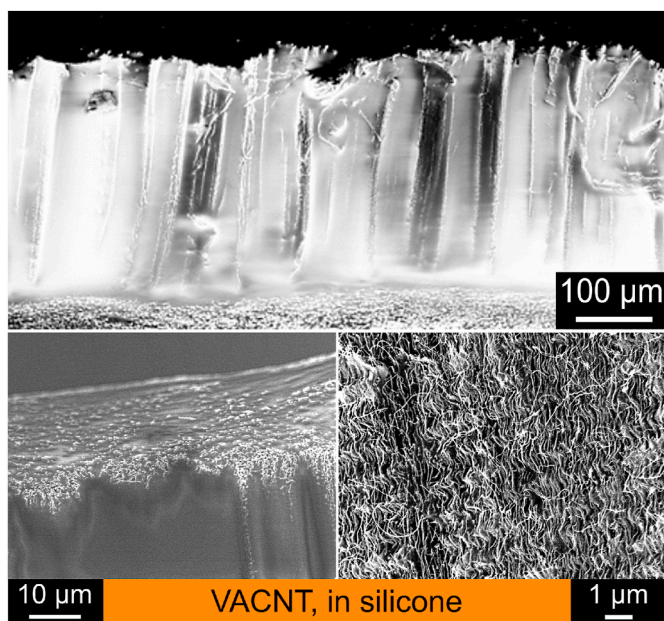


Fig. 4. Electron microscopy images of a silicone film containing VACNT (DC = 738). The high charging of the film indicates that the CNTs are fully embedded into an insulator, the silicone. (see also the EDX measurement in the Supplementary Information, figure SI5).

resulting in the formation of CF-CNTs. On the way to the high number of laser pulses, i.e. DC, the beginning of the CF-CNT-formation is observed as small entanglements on the surface layer (Pre-CF-CNTs) (Fig. 1c), while finally massive entangled CNT pads are formed as seen in Fig. 1d (more images are found in Supplementary Information Fig. SI1).

The particle density reaches an optimal value for VACNT growth at 738 DCs for the given laser parameters (Fig. 2a). The morphology of the catalytic nanoparticles is shown in Fig. 2b.

The multi-walled VACNTs have an averaged diameter of about 20–25 nm, corresponding to about 30 layers [22] (see Supplementary Information Fig. SI2). The thermogravimetric analysis confirms the very low metal content of 0.7% w/w indicating that the catalytic nanoparticles stay at the surface during CNT growth (top-growth) (see

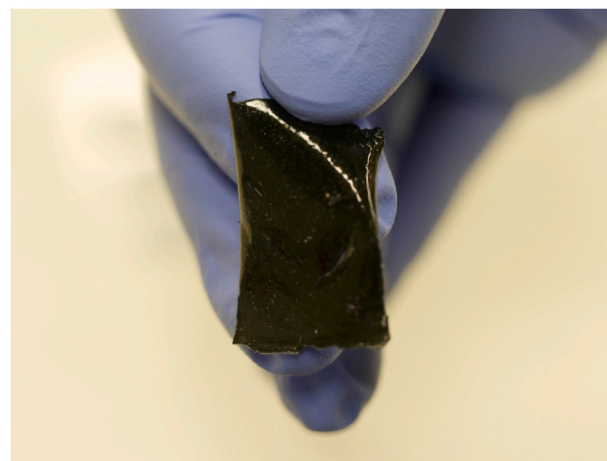


Fig. 5. Silicone/CNT film (DC = 711) released from the substrate.

Supplementary Information Fig. SI3).

The reflection spectra of the various CNT morphologies are shown in Fig. 3, together with two commercially available black carbon-based acrylic paints, Black 1.0 and Black 3.0.

The lowest reflection of 0.5–1.0% at all wavelengths in the range from 200 nm to 2300 nm is obtained for Pre-VACNTs, followed by VACNTs. Pre-CF-CNT, as well as CF-CNTs, show a higher reflection rate across all wavelengths. The orientation of the CNTs relative to a light source, as well as the morphology of the CNT coating itself, has a massive influence on the absorption properties of the nanostructured surface. Individual nanotubes show only a weak interaction with light incident parallel to the long axis of the tube because its electrons cannot couple with the electric field of the light [23]. Therefore, VACNT-surfaces show relatively low reflection values and a high transmission rate into the CNT ‘forest’, where light trapping occurs inside the cavities of the structure, while it either gets absorbed from the CNTs or reflected between the individual CNT until it gets absorbed. Optimal light trapping occurs at 20° incidence angle of the light relative to the tube axis [19]. For partially stabilized Pre-VACNTs this condition is more often fulfilled over the whole surface than for VACNTs, making them an even better absorber for vertically incident light. The acrylic

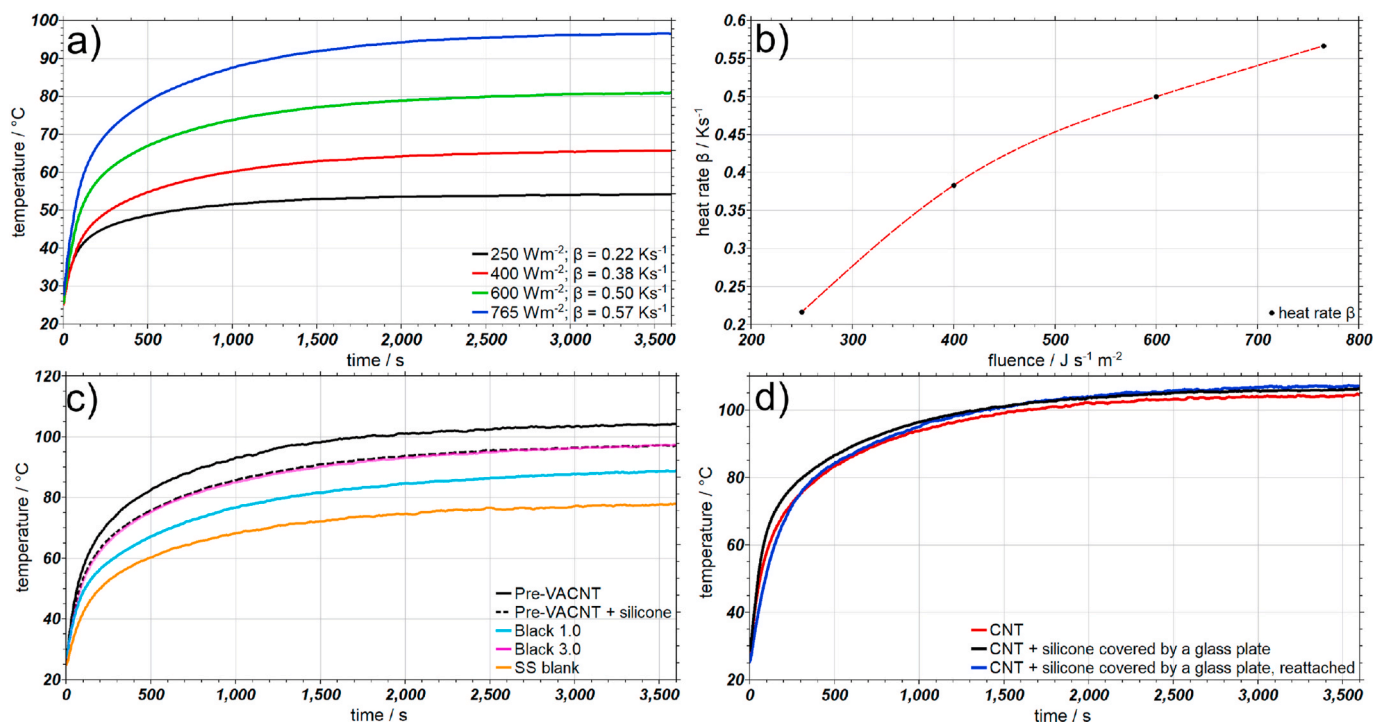


Fig. 6. Light-induced temperature increase. a) Temperature increase and b) initial heating rate β (slope measured 10 s after the start of illumination) depending on the used radiation intensity (VACNT, DC = 767), c) comparison of Pre-VACNT arrays (DC = 711, $\Phi = 765 \text{ W cm}^{-2}$) with and without silicone soaking, with blank stainless steel, Black 1.0 and 3.0 as references. d) silicone/CNT film as-grown (red), covered with a glass plate (black), and after removal and reattachment, again with a glass plate on top (blue). (In the Supplementary Information more heating curves for other DC values are shown in figure SI6.). (For interpretation of the references to colour in this figure legend, the reader is referred to the Web version of this article.)

paints Black 1.0 and 3.0 show comparably low reflection in the visible like the VACNTs, however, much higher reflection in the UV- and in particular the IR-region.

The narrow packing of CNTs causes strong capillary effects, enabling them to easily suck up even relatively viscose fluids like a silicone prepolymer. The following hardening of the silicone by cross-linking does not disturb the alignment of the CNTs (Fig. 4).

The silicone films are prepared to allow easy handling as they show good mechanical stability. They can be detached from the steel substrate required for its preparation (Fig. 5) fully preserving its internal structure and anisotropic properties. The films may be attached to merely every sample by air pressure, due to their smooth and soft surface.

We checked the properties of the CNT films by testing their light-to-heat conversion (Fig. 6).

The heating rate, as well as the steady-state temperature increase, is almost linearly dependent on the radiation fluence (Fig. 6a and b). Comparing the temperature increase after a 1-h exposure, i.e. in the steady-state caused by a light fluence of $\Phi = 765 \text{ W m}^{-2}$, it can be seen, that silicone soaking of the VACNT array leads to slightly lower heating because of the somewhat higher reflection of the silicone film (please refer to the Supplementary Information SI4). The temperature decrease of around 7.5 °C, which is shown for Pre-VACNTs in Fig. 6c, matches the temperature curve of Black 3.0. The CNT coated sample reaches a more than 25 °C higher steady-state temperature and the silicone/CNT sample still an about 20 °C higher temperature than the reference, the untreated blank stainless steel sample.

To test the preservation of the light-to-heat conversion properties after removing the film from the substrate and reattaching it onto another sample, it was tested with a glass plate on top which was required to press the detached CNT film onto the new surface (Fig. 6d). First, the covering glass plate causes a slight increase of the steady-state temperature because the heat convection to air is suppressed and fully resembles the properties of the CNT film without silicone, and second,

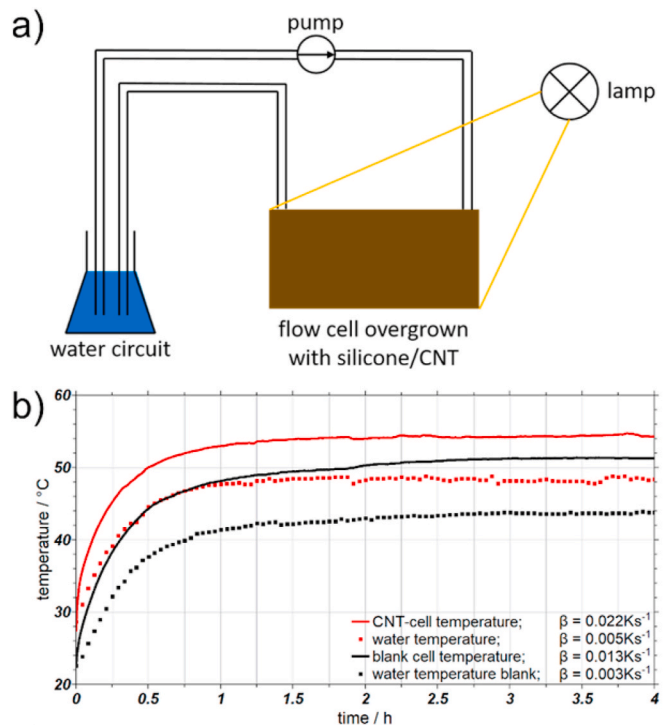


Fig. 7. Dynamic measurement of radiation-induced temperature increase. a) Scheme of the used setup. b) Radiation-induced temperature increase for a flow cell covered with a silicone/Pre-VACNT film and a blank stainless steel flow cell as reference. The initial heating rate β was measured 10 s after the beginning of the illumination.

there is no loss in performance of the reattached silicone/CNT film proving that it can be transferred to any other surface without any losses.

CNTs are known for their anisotropic heat conduction, strongly favoring heat transfer along their long axis [24]. Therefore, VACNTs should provide an increased heat transfer from the CNT layer to the metallic plate. The heat conductance properties are mainly interesting where two objects of different temperatures are connected by a silicone/VACNT film, e.g., a microprocessor and a cooling device.

We tested the heat transfer from the CNT film itself to its substrate and further on to e.g. water. For dynamic temperature measurements, flow cells with a capacity of 0.8 mL were prepared. A total volume of 30 mL (37.5-times the volume of the capacity of the cell) water was pumped with a flow rate of 35 mL min⁻¹ (1.17-times exchange of the total volume per minute) through the cells. For both a blank stainless steel cell, as well as for a silicone/Pre-VACNT overgrown cell the temperature was measured directly at the bottom of the flow cell, as well as in the water circuit (Fig. 7).

Dynamic measurements result in heat rate differences between the two samples. The CNT coated cell shows a 40% higher heat rate of $\beta = 0.022 \text{ K s}^{-1}$ compared to the blank cell with $\beta = 0.013 \text{ K s}^{-1}$. Also in the steady-state, the flow cell, as well as the water reservoir, reach temperatures a few degrees higher than without the CNT coating (Fig. 7b).

4. Conclusions

Silicone/CNT hybrid films have been prepared on stainless steel substrates for various CNT architectures, VACNT as well as CF-CNT. Reflection spectra for the different CNT-morphologies show their very high light absorbance with Pre-VACNT and VACNT films having the lowest reflections in the whole range from 200 to 2300 nm. Soaking with silicone and crosslinking supplies flexible films without losing their internal anisotropic alignment and therefore their anisotropic heat conductance in the case of VACNTs when they are removed from the substrates. As tests heat conversion from (sun)light was used. Due to the slightly higher reflection of the silicone films, the induced temperature decreases after 1 h by 8 °C on average across all examined samples at an illumination of $\Phi = 765 \text{ J s}^{-1}\text{m}^{-2}$. This means that the test samples reached not 100 °C but 92 °C under the conditions applied. For dynamic measurements with a water circuit, silicone/CNT samples show a 40% higher heating rate compared to untreated samples of stainless steel. Temperature rise curves of the attached and reattached silicone/CNT films show that the function of the silicone films is fully preserved. This finding enables to separate CNT preparation and their use because the produced silicone/CNT films can be transferred to any other surface without any functional loss.

CRedit authorship contribution statement

Michael Dasbach: The manuscript was written through the contributions of all authors. All authors have approved the final version of the manuscript. **Norbert A. Hampp:** The manuscript was written through the contributions of all authors. All authors have approved the final version of the manuscript.

Declaration of competing interest

The authors declare that they have no known competing financial interests or personal relationships that could have appeared to influence the work reported in this paper.

Acknowledgments

We thank D. Renz for the mirror-polishing of the homemade flow cells.

Appendix A. Supplementary data

Supplementary data to this article can be found online at <https://doi.org/10.1016/j.matchemphys.2021.124690>.

Funding

This research did not receive any specific grant from external funding agencies in the public, commercial, or not-for-profit sectors.

References

- [1] A.V. Radhamani, H.C. Lau, S. Ramakrishna, CNT-reinforced metal and steel nanocomposites: a comprehensive assessment of progress and future directions, *Compos. Appl. Sci. Manuf.* 114 (2018) 170–187, <https://doi.org/10.1016/j.compositesa.2018.08.010>.
- [2] W.A. Curtin, B.W. Sheldon, CNT-reinforced ceramics and metals, *Mater. Today* 7 (2004) 44–49, [https://doi.org/10.1016/S1369-7021\(04\)00508-5](https://doi.org/10.1016/S1369-7021(04)00508-5).
- [3] S.I. Yengejeh, S.A. Kazemi, A. Öchsner, Carbon nanotubes as reinforcement in composites: a review of the analytical, numerical and experimental approaches, *Comput. Mater. Sci.* 136 (2017) 85–101, <https://doi.org/10.1016/j.commatsci.2017.04.023>.
- [4] Y. Li, Y. Liu, N. Hu, Reinforcement effects on CNTs for polymer-based nanocomposites, in: S. Yellampalli (Ed.), *Carbon Nanotubes – Polymer Nanocomposites*, Tech, Rijeka, 2011, pp. 129–154, <https://doi.org/10.5772/19605>.
- [5] A.T. Sepúlveda, R. Guzman de Villoria, J.C. Viana, A.J. Pontes, B.L. Wardle, L. A. Rocha, Full elastic constitutive relation of non-isotropic aligned-CNT/PDMS flexible nanocomposites, *Nanoscale* 5 (2013) 4847–4854, <https://doi.org/10.1039/c3nr00753g>.
- [6] Y.J. Jung, S. Kar, S. Talapatra, C. Soldano, G. Viswanathan, X. Li, Z. Yao, F.S. Ou, A. Avadhanula, R. Vajtai, S. Curran, O. Nalamasu, P.M. Ajayan, Aligned carbon nanotube-polymer hybrid architectures for diverse flexible electronic applications, *Nano Lett.* 6 (2006) 413–418, <https://doi.org/10.1021/nl052238x>.
- [7] E.A. Taft, H.R. Philipp, Optical properties of graphite, *Phys. Rev.* 138 (1965) 197–202, <https://doi.org/10.1103/PhysRev.138.A197>.
- [8] J. Appenzeller, J. Knoch, V. Derycke, R. Martel, S. Wind, P. Avouris, Field-modulated carrier transport in carbon nanotube transistors, *Phys. Rev. Lett.* 89 (4) (2002) 126801, <https://doi.org/10.1103/PhysRevLett.89.126801>.
- [9] Y.F. Li, T. Kaneko, J. Kong, R. Hatakeyama, Photoswitching in azafullerene encapsulated single-walled carbon nanotube FET devices, *J. Am. Chem. Soc.* 131 (2009) 3412–3413, <https://doi.org/10.1021/ja810086g>.
- [10] Y. Miyauchi, M. Iwamura, S. Mouri, T. Kawazoe, M. Ohtsu, K. Matsuda, Brightening of excitons in carbon nanotubes on dimensionality modification, *Nat. Photonics* 7 (2013) 715–719, <https://doi.org/10.1038/nphoton.2013.179>.
- [11] Y. Miyauchi, Photoluminescence studies on exciton photophysics in carbon nanotubes, *J. Mater. Chem. C* 1 (2013) 6499–6521, <https://doi.org/10.1039/C3TC00947E>.
- [12] C.W. Chen, M.H. Lee, S.J. Clark, Band gap modification of single-walled carbon nanotube and boron nitride nanotube under a transverse electric field, *Nanotechnology* 15 (2004) 1837–1843, <https://doi.org/10.1088/0957-4484/15/12/025>.
- [13] T. Durkop, S.A. Getty, E. Cobas, M.S. Fuhrer, Extraordinary mobility in semiconducting carbon nanotubes, *Nano Lett.* 4 (2004) 35–39, <https://doi.org/10.1021/nl034841q>.
- [14] M. Kanungo, H. Lu, G.G. Malliaras, G.B. Blanchet, Suppression of metallic conductivity of single-walled carbon nanotubes by cycloaddition reactions, *Science* 323 (2009) 234–237, <https://doi.org/10.1126/science.1166087>.
- [15] A. Cao, X. Zhang, X. Xu, B. Wei, D. Wu, Tandem structure of aligned carbon nanotubes on Au and its solar thermal absorption, *Sol. Energy Mater. Sol. Cells* 70 (2002) 481–486, [https://doi.org/10.1016/S0927-0248\(01\)00083-6](https://doi.org/10.1016/S0927-0248(01)00083-6).
- [16] J.Q. Xi, M.F. Schubert, J.K. Kim, E.F. Schubert, M. Chen, S.Y. Lin, W. Liu, J. A. Smart, Optical thin-film materials with low refractive index for broadband elimination of Fresnel reflection, *Nat. Photonics* 1 (2007) 176–179, <https://doi.org/10.1038/nphoton.2007.26>.
- [17] M. Gershow, J.A. Golovchenko, Recapturing and trapping single molecules with a solid-state nanopore, *Nat. Nanotechnol.* 2 (2007) 775–779, <https://doi.org/10.1038/nnano.2007.381>.
- [18] C. Lee, S.Y. Bae, S. Mobasser, H. Manohara, A novel silicon nanotips antireflection surface for the micro sun sensor, *Nano Lett.* 5 (2005) 2438–2442, <https://doi.org/10.1021/nl0517161>.
- [19] K. Mizuno, J. Ishii, H. Kishida, Y. Hayamizu, S. Yasuda, D.N. Futaba, M. Yumura, K. Hata, A black body absorber from vertically aligned single-walled carbon nanotubes, *Proc. Natl. Acad. Sci. Unit. States Am.* 106 (15) (2009) 4, <https://doi.org/10.1073/pnas.0900155106>.
- [20] H. Reinhardt, C. Hellmann, P. Nürnberger, S. Kachel, N. Hampp, Freeform growth of carbon nanotube microarchitectures on stainless steel controlled via laser-stimulated catalyst formation, *Adv. Mat. Interfaces* 4 (2017), <https://doi.org/10.1002/admi.201700508>, 1700508/1-1700508/7.
- [21] M. Dasbach, M. Pyschik, V. Lehmann, K. Parey, D. Rhinow, H. Reinhardt, N. Hampp, Assembling carbon nanotube Architectures, *ACS Nano* 14 (2020) 8181–8190, <https://doi.org/10.1021/acsnano.0c01606>.

- [22] C. Hierold (Ed.), Carbon Nanotube Devices – Properties, Modeling, Integration and Applications, Wiley, Weinheim, 2008, ISBN 978-3-527-31720-2.
- [23] Y. Murakami, E. Einarsson, T. Edamura, S. Maruyama, Polarization dependence of the optical absorption of single-walled carbon nanotubes, Phys. Rev. Lett. 94 (2005) 2664–2676, <https://doi.org/10.1016/j.carbon.2005.05.036>.
- [24] J. Chen, L. Wang, X. Gui, Z. Lin, X. Ke, F. Hao, Y. Li, Y. Jiang, Y. Wu, X. Shi, L. Chen, Strong anisotropy in thermoelectric properties of CNT/PANI composites, Carbon 114 (2017) 1–7, <https://doi.org/10.1016/j.carbon.2016.11.074>.